chemosensors

MDPI

Article

Thiol-Amine Functionalized Decorated Carbon Nanotubes for Biomarker Gases Detection

Atef Thamri [1], Hamdi Baccar [1], Juan Casanova-Chafer [2], Moataz Billeh Mejri [1], Eduard Llobet [2,*] and Adnane Abdelghani [1]

[1] Research Unit of Nanobiotechnology and Valorisation of Medicinal Phytoressources UR17ES22, National Institute of Applied Science and Technology, University of Carthage, Centre Urbain Nord, Charguia 1080, CEDEX Bp 676, Tunisia; atef.thamri@fst.utm.tn (A.T.); hamdibaccar@gmail.com (H.B.); moataz.billeh.mejri@hotmail.fr (M.B.M.); adnane.abdelghani@insat.rnu.tn (A.A.)

[2] Department of Electronics Engineering, Universitat Rovira i Virgili, MINOS, 43007 Tarragona, Spain; juan.casanova@urv.cat

* Correspondence: eduard.llobet@urv.cat

Abstract: Thousands of gas molecules are expelled in exhaled breath, and some of them can reveal diseases and metabolomic disorders. For that reason, the development of fast, inexpensive, and reliable sensing devices has been attracting growing interest. Here, we present the development of different chemoresistors based on multi-walled carbon nanotubes (MWCNTs) decorated with platinum (MWCNT/Pt) and palladium (MWCNT/Pt) nanoparticles and also functionalized with a self-assembled monolayer (SAM) of 11-amino-1-undecanethiol (Thiol-amine). The nanocomposites developed are a proof-of-concept to detect some biomarker molecules. Specifically, the capability to identify and measure different concentrations of volatile organic compounds (VOCs), either aromatic (toluene and benzene) and non-aromatic (ethanol and methanol) was assessed. As a result, this paper reports the significant differences in sensing performance achieved according to the metal nanoparticle used, and the high sensitivity obtained when SAMs are grown on the sensitive film, acting as a receptor for biomarker vapours.

Keywords: carbon nanotubes; metal decoration; self-assembled monolayer; thiol-amine; gas sensing; biomarkers detection

Citation: Thamri, A.; Baccar, H.; Casanova-Chafer, J.; Mejri, M.B.; Llobet, E.; Abdelghani, A. Thiol-Amine Functionalized Decorated Carbon Nanotubes for Biomarker Gases Detection. *Chemosensors* **2021**, *9*, 87. https://doi.org/10.3390/chemosensors9050087

Academic Editor: Marc Debliquy

Received: 23 March 2021
Accepted: 21 April 2021
Published: 23 April 2021

1. Introduction

Exhaled breath is a complex matrix in which many molecules can be present, constituting a "breath-print" that can provide information about health issues [1]. In consequence, many research efforts have been focused on the development of non-invasive sensing devices to detect the presence of biomarkers in exhaled breath [2]. Many techniques are available to analyse exhaled breath samples, such as gas chromatography, which consists of the vaporization of the collected sample and the separation (through a series of columns) of the different compounds present in the matrix for their identification [3]. This technique is extremely sensitive and accurate, but the main problems that are preventing its effective implementation are the high cost of analysis, poor miniaturization, and lack of portability [4–6]. Other alternative techniques are optical methods (e.g., fluorescence and surface enhanced Raman spectroscopy) that provide reliable and selective readouts, but their high cost, the need for skilled personnel, and limited portability are still an issue [7,8].

Nevertheless, during the last few years chemical resistive (chemoresistive) gas sensors have been researched as a feasible option to obtain breath-prints [9]. This type of device offers a straightforward working principle, in which the interaction of the gas compounds with the sensitive film is translated into a change in the electrical resistance [10]. Chemoresistors present some benefits over other alternatives, such as inexpensiveness, high portability, simple driving and readout circuitry, and are suitable for achieving real-time results [11]. However, some issues remain a challenge, such as poor standardization

and selectivity [12,13]. For that reason, despite the great research efforts focused on the development of sensitive nanomaterials, a growing number of studies are trying to create multivariable sensing platforms [11]. With this approach, an array of different gas sensors can be developed for discriminating target gas molecules in a matrix, and therefore reducing cross-interferences [9]. Indeed, during the last few years, the use of electronic noses has become a thriving option [14]. These analytical devices comprise a sensor array with partially overlapping selectivity and have been reported to be useful for detecting some disease biomarkers in breath samples for diagnosing the early stages of lung cancer [15,16], chronic obstructive pulmonary disease (COPD) [17], or cystic fibrosis [18]. Not limited to exhaled breath, electronic noses have also been employed for urine analysis and the detection of biomarkers that may reveal the presence of several health issues, such as prostatic cancer [19] or bile acid diarrhoea [20].

Nowadays, nanotechnology makes possible producing sensor devices based on nanomaterials such as carbon nanotubes, metal nanoparticles, and self-assembled monolayers. Carbon nanotubes, discovered in 1991 by Iijima [21], have a high potential to become used as gas sensitive materials since they can now be produced at low cost [22–26]. The physical and chemical modification of carbon nanotubes has become an important area of research in recent years, in order to increase their performance and applicability. These modifications of CNTs have made it possible to improve their solubility in aqueous media and in organic solvents [27], which has made it possible to use CNTs in different fields. Several methods of modifying CNTs have been used, particularly by substitutive doping [28–30], by grafting functional groups on the outer wall of the tubes by wet chemical or reactive plasma [31–33] and/or by decorating their surface using a wide range of materials such as metal oxide nanoparticles [34–38], polymers [39–42], non-polymeric organic materials [43–45] or nanoparticles (such as Rh, Pd, Pt or Au) [46–50]. All these modifications can be used for tuning sensitivity and selectivity, and thus, help meeting the requirements of different gas sensing applications [51–53]. In addition, gas sensing devices employing carbon nanotubes can be operated at room temperature [46–48], which makes them attractive for any application in which power consumption is an issue, such as in portable, battery operated devices or in wireless sensing networks.

The main novelty of this work lies on the functionalization of oxygen plasma treated MWCNTs with self-assembled monolayers (SAM) of 11-amino-1-undecanethiol and the study of their gas sensing properties. Several chemoresistors are developed employing multiwalled carbon nanotube films decorated with platinum (MWCNT/Pt) and palladium (MWCNT/Pd) nanoparticles, functionalized with a thiol-amine SAM, designated as MWCNT/Pt/thiol-amine and MWCNT/Pd/thiol-amine. The effect of having amine functional groups on the detection of vapours from aromatic and non-aromatic volatile organic compounds is studied. In addition, it is known that the hydrophobic nature of the amine functional would help to reduce moisture cross-sensitivity in these hybrid nanomaterials. The SAM technique has been used regularly for many years in biosensor applications [54,55]. This technique relies on the good affinity existing between the reactive sulphur group present at one end of the thiol-amine molecule and metal nanoparticles (Pt and Pd), which decorate the outer wall of carbon nanotubes. Transmission electron microscopy (TEM) and the Fourier-transform infrared spectroscopy (FTIR) characterizations were carried out to analyse the chemical and structural composition of the sensitive films and to check the feasibility of the functionalization. Then, the different gas sensors were employed to detect either aromatic and non-aromatic VOCs.

It is well-known that hundreds of different VOCs can be present in human breath [56], indicating the state of health and the possible presence of some diseases or metabolomic disorders [57]. For that reason, the sensing performance of the different sensitive films developed was assessed towards four VOCs that are considered biomarkers. Specifically, two aromatic compounds (benzene and toluene) and other two non-aromatic (ethanol and methanol) were selected as target gas molecules. All of them are associated with several health issues. For instance, the presence of benzene and toluene in exhaled breath (at

hundreds of ppb levels) derived from the exposure to tobacco smoke (even second-hand exposure) is associated with a greater risk of lung cancer and other pulmonary pathologies [58]. Meanwhile, ethanol is linked to bacterial metabolism and obesity-related fatty liver [59]. Therefore, high levels of ethanol in human breath (at units of ppm levels) may reveal a higher risk of obesity and non-alcoholic steatohepatitis (NASH) [59]. Regarding methanol detection, this is a usual compound present in exhaled breath due to the colonic microbial production derived from unabsorbed complex carbohydrates [60]. However, the increase in methanol concentration in breath may indicate other health issues. For instance, aspartame is widely used as a sweetener in foods and beverages, and methanol is one of the resulting compounds derived from aspartame hydrolysis in the gastrointestinal tract. Then, a high concentration of methanol in the exhaled breath (at ppm levels) may indicate a high-aspartame diet, which may cause several health problems like a higher risk for diabetes or obesity [61].

Nonetheless, if the ultimate goal was the effective detection of specific diseases such as lung cancer, instead of merely identifying patients at higher risk of suffering health issues, this would require the simultaneous detection and quantification of several biomarkers (i.e., fingerprint analysis). By performing such an analysis, correlation coefficients and their corresponding *p*-values can be calculated for diagnosing a specific disease [62]. For instance, the exhaled breath of lung cancer (LC) patients tends to show a lower relative concentration of methanol than that of healthy volunteers [63]. Conversely, benzene and toluene show higher relative abundance in LC patients [64,65].

2. Materials and Methods

2.1. Synthesis and Decoration of Carbon Nanotubes

The multi-walled carbon nanotubes (MWCNT) were purchased from Nanocyl S.A. (Belgium). These nanotubes were synthesized by chemical vapour deposition (CVD method) [66] and purity greater than 95%. The length of the nanotubes is approximately 50 μm and their inner and outer diameters are 3 to 15 nm, respectively. Since the dispersion and reactivity of the surface of the nanotubes are relatively low, homogeneous oxygen functionalization has been carried out to the MWCNTs. During this step, reactive sites (i.e., oxygen vacancies) appear on the outer walls of MWCNTs, in which metal nanoparticles can be nucleated during the sputtering process. The method of functionalization of MWCNTs which has been applied is based on plasma treatment of oxygen [67]. To perform this, the MWCNTs were placed in a glass vessel located in the plasma chamber. Then, the MWCNT powder underwent stirring through the effect of a magnet located outside to ensure homogeneous functionalization. As soon as the powder of the MWCNTs was placed inside the chamber, a controlled flow of a mixture of oxygen and argon was introduced to promote the attachment of the functional oxygenated groups to the MWCNTs surface [68]. The treatment was performed by an inductively coupled plasma at an RF frequency of 13.56 MHz, at low pressure (0.1 Torr), and using a power of 15 W. The processing time was optimized at 1 min [47].

Once the functionalizing step was properly performed, a 0.1 mg/mL MWCNT solution was prepared in dimethylformamide (DMF). Thereafter, the solution was placed in an ultrasonic bath for 20 min at room temperature to achieve a suitable dispersion of the carbon nanotubes in the solvent. Subsequently, the dispersed MWCNTs were deposited on the interdigitated electrode area of the sensor substrates by airbrushing, which is a mechanical deposition process using nitrogen as a carrier gas. Commercially available alumina substrates from Ceram Tech GmbH (Plochingen, Germany) were used. These comprise screen-printed, interdigitated platinum electrodes (300 μm gap) on their front side and an 8 Ω screen-printed Pt heater on their backside. During airbrushing, the sensor substrate was kept at 100 °C for achieving fast evaporation of the solvent. In addition, the resistance of the device was monitored during the process, which was conducted until sensor resistance reached 5 kΩ. This enables us to control both the density of the CNT coating and the amount of MWCNTs deposited, ameliorating device to device reproducibility. After the

deposition phase, the MWCNTs were decorated with metal nanoparticles by sputtering (ATC Orion 8-HV-AJA International, North Scituate, MA, USA). This technique consists of bombarding the surface of a metallic disc with a plasma beam. Therefore, nanoparticles cling to the walls of MWCNTs under the effect of nucleation, achieving the MWCNTs' decoration. Besides, the presence of defects and oxygenated functional groups grafted at the outer walls facilitates the immobilization of the nanoparticles, avoiding some well-known problems such as coalescence [11]. The power and time required for the plasma beam aperture within the cell were optimized and are shown in Table 1 for both types of metal nanoparticles. The optimization of these sputtering parameter values was conducted for achieving a similar, homogeneous loading of the surface of MWCNTs with either Pt or Pd nanoparticles of similar size. According to previous results, the loading of MWCNTs with either Pd or Pt is near 2% in weight [46,49]. In total four sensors loaded with Pt and another four loaded with Pt were prepared. Two sensors of each type were further functionalised with thiol-amine.

Table 1. Sputtering experimental conditions applied for MWCNT decoration.

Material	Power (W)	Time (s)
Platinum	150	14
Palladium	30	8

2.2. Deposition of Self-Assembled Monolayers (SAMs)

SAM functionalization was carried out on the surface of Pt and Pd nanoparticles by using monolayers of 11-amino-1-undecanethiol (Thiol-amine). The MWCNTs decorated with nanoparticles were immersed in 1 mM of thiol amine diluted in ethanol for 24 h at 4 °C. Then, the sensors were rinsed with ethanol and dried under a nitrogen stream. This procedure was repeated 3 times to remove thiol residues not attached to metal nanoparticles [69]. Figure 1 depicts the synoptic structure of the sensor before and after the thiol amine deposition.

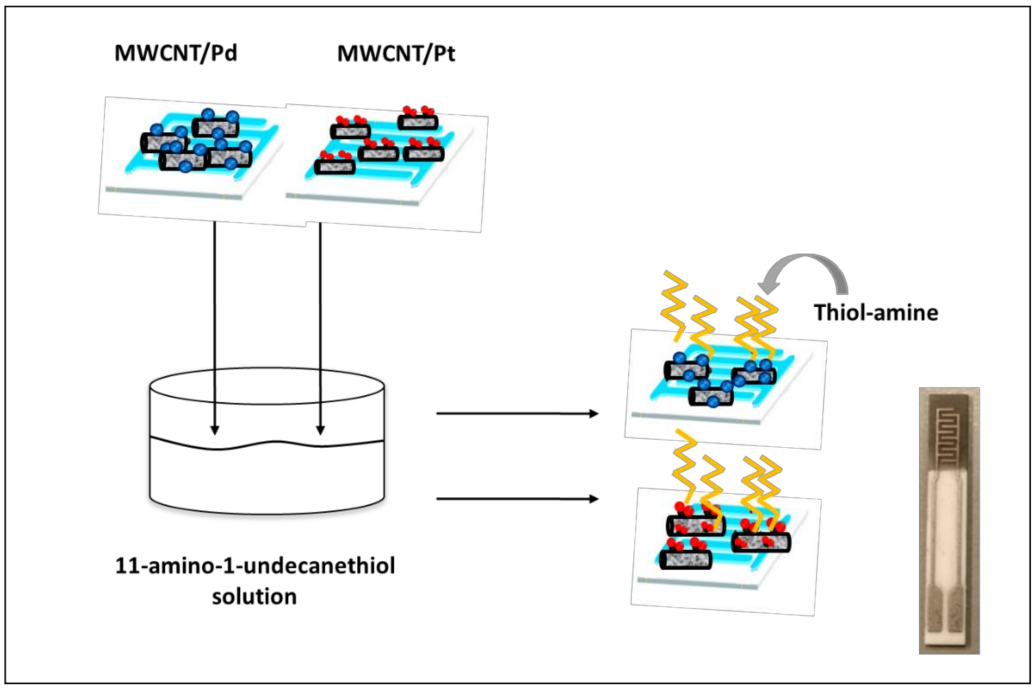

Figure 1. Synoptic structure of the sensor before and after thiol amine deposition. The image on the bottom right shows the front face of a sensor. The dark area over the interdigitated electrodes is the SAM-functionalised MWCNT film.

2.3. Characterization Techniques

Morphological characterization of the MWCNTs decorated by Pt and Pd nanoparticles was conducted by using a transmission electron microscope (TEM model JEOL 1011, Akishima, Japan) operated at 100 kV. This technique enables the assessment of the quantity and distribution of the metallic nanoparticles attached to the MWCNTs.

Atomic force microscope (AFM) images were obtained by using our MFP-3D Origin type from Oxford Instruments (Abingdon-on-Thames, UK). These images were recorded in tapping mode [70]. This technique allows the direct visualization of the sensor surface and evaluates the quality of the sensitive layer deposited on the substrates.

Finally, an Alpha FTIR spectrometer (Bruker, Billerica, MA, US) equipped with an ATR Platinum crystal diamond module was employed to obtain information about the structure and growth of SAMs. These infrared spectra were obtained in absorbance mode.

2.4. Gas Sensing Measurements

The different sensors developed were tested for the detection of aromatic VOCs (toluene and benzene, 99.8% pure, purchased from Sigma Aldrich, St. Louis, MO, USA) and non-aromatic gases (ethanol and methanol, 99.5% pure, purchased from Sigma Aldrich). These species are susceptible to be biomarkers of several diseases as was mentioned before.

The vapours were generated by a dilution bench consisting of a chemical vaporization cell of the solvents and two flowmeters (Brook Instruments, Hatfield, PA, USA) to generate reproducible concentrations of the different vapours tested. Zero grade dry air was used for dilution and as carrier gas (Air Liquide, ZI Charguia, Tunisia). These were coupled to a sensor cell (35 cm^3 volume) which can hold up to 6 sensors at the same time. Sensor resistance was measured by using an Agilent HP 34972A multimeter. Figure 2 illustrates the experimental set-up used. All measurements were carried out in pure dry air, at ambient temperature, under a constant flow of 100 cm^3/min. Under these conditions, relative humidity inside the test chamber was 5% at 24 °C. The response of the sensors was defined as the normalized resistance variation, summarized in the following equation:

$$\Delta R/R_0\ (\%) = [(R_g - R_0)/R_0)] \times 100$$

where R_g and R_0 are the resistance under the VOCs compounds and dry air, respectively.

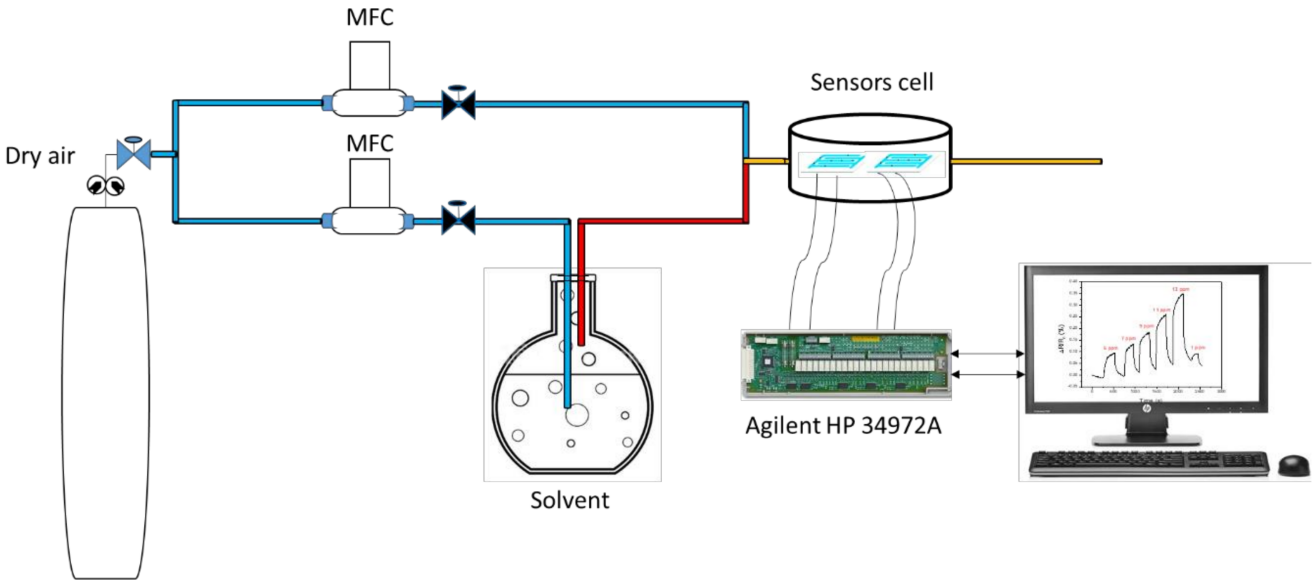

Figure 2. Sketch of the experimental set-up used to characterize gas sensing properties.

3. Results

3.1. Material Characterization

3.1.1. Transmission Electron Microscopy (TEM)

In order to carry out the TEM characterization, MWCNTs were suspended in ethanol and then deposited on a copper grid. Figure 3 shows that the Pd and Pt nanoparticles were successfully and homogeneously grafted onto the sidewalls of the MWCNTs. Figure 3a shows the TEM analysis performed on the MWCNTs/Pd sensor film with an average nanoparticle size of about 1.5 ± 0.1 nm. The analyses on the film MWCNTs/Pt (Figure 3b) show that the average size of the nanoparticles is 1.0 ± 0.1 nm. The size of Pt and Pd nanoparticles was estimated by taking TEM micrographs of the Pt and Pd loaded MWCNT samples and averaging the size of 50 nanoparticles.

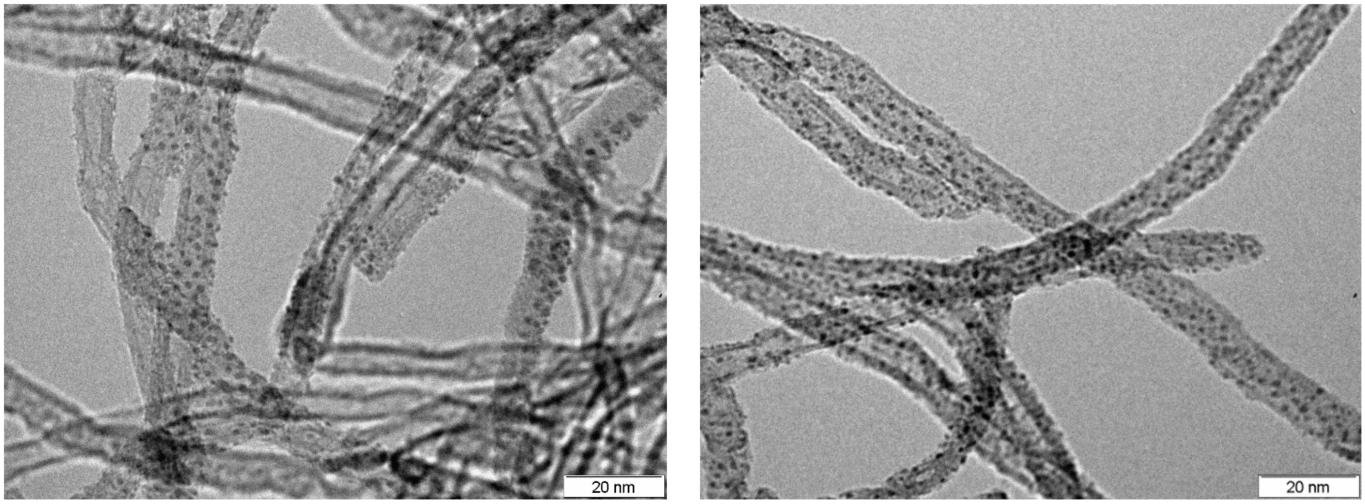

Figure 3. TEM images of MWCNTs decorated with palladium (**a**) and platinum (**b**) nanoparticles.

3.1.2. Atomic Force Microscopy (AFM)

Figure 4 shows a typical AFM image of a MWCNT/Pd film, already deposited on the alumina substrate. This analysis was carried out in order to verify the success of the deposition of the MWCNTs on the substrate. The AFM analyses performed on decorated carbon nanotube film (MWCNTs/Pt or Pd) did not show the presence of Pt nor Pd nanoparticles. This is because the resolution of the AFM instrument used is not enough for observing nanoparticles under 3 nm in size, which is the case here, as revealed by TEM. What the AFM analysis shows is the elongated structure of MWCNTs and that airbrushed films on the alumina sensor substrates consist of homogeneous and porous mats of MWCNTs. The dark sections in the micrograph correspond to voids into which vapours will easily diffuse.

3.1.3. Fourier-Transform Infrared Spectroscopy (FTIR)

FTIR characterization was used to study/confirm the formation and immobilization of thiol-amine monolayers on the MWCNTs/Pd and MWCNTs/Pt films. Figure 5 shows the infrared spectra in absorbance mode, in which the wavenumbers range from 500 cm^{-1} to 4000 cm^{-1}. Specifically, Figure 5a compares the MWCNTs/Pd/Thiol-amine and MWCNTs/Pd spectra, while Figure 5b compares the MWCNTs/Pt/Thiol-amine and MWCNTs/Pt spectra.

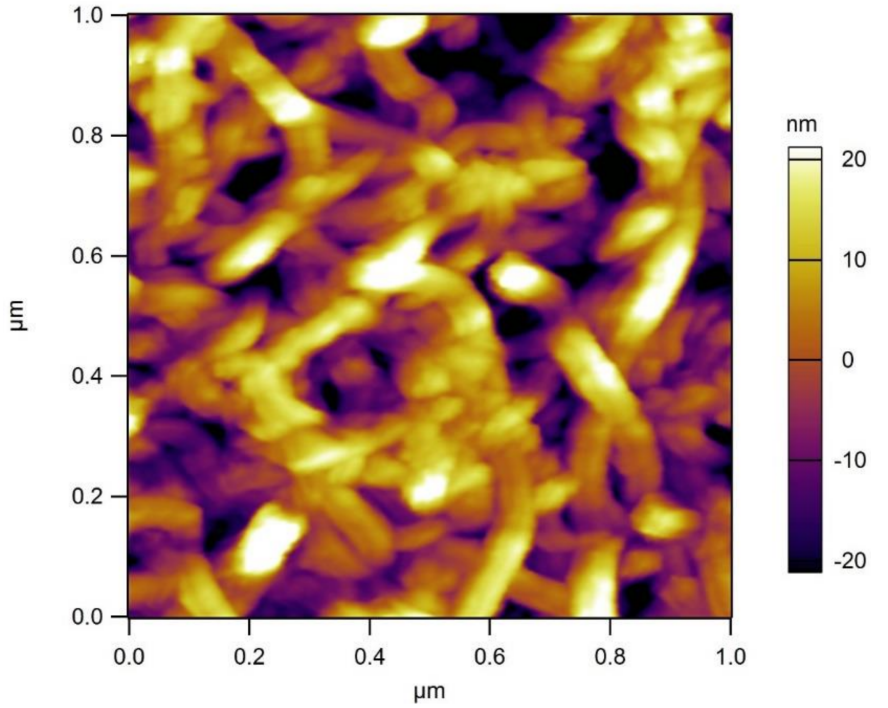

Figure 4. Typical AFM image for an airbrushed MWCNT/Pd film deposited on an alumina substrate.

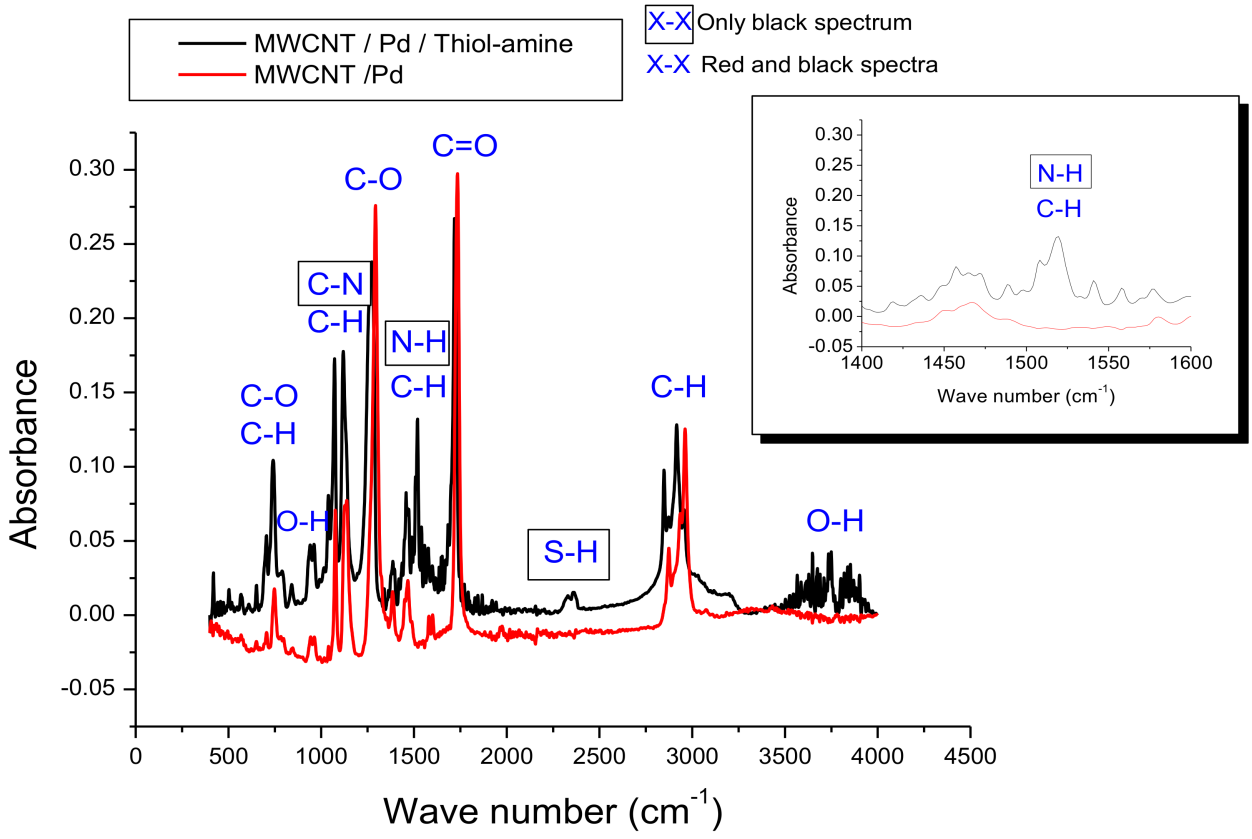

(**a**)

Figure 5. *Cont.*

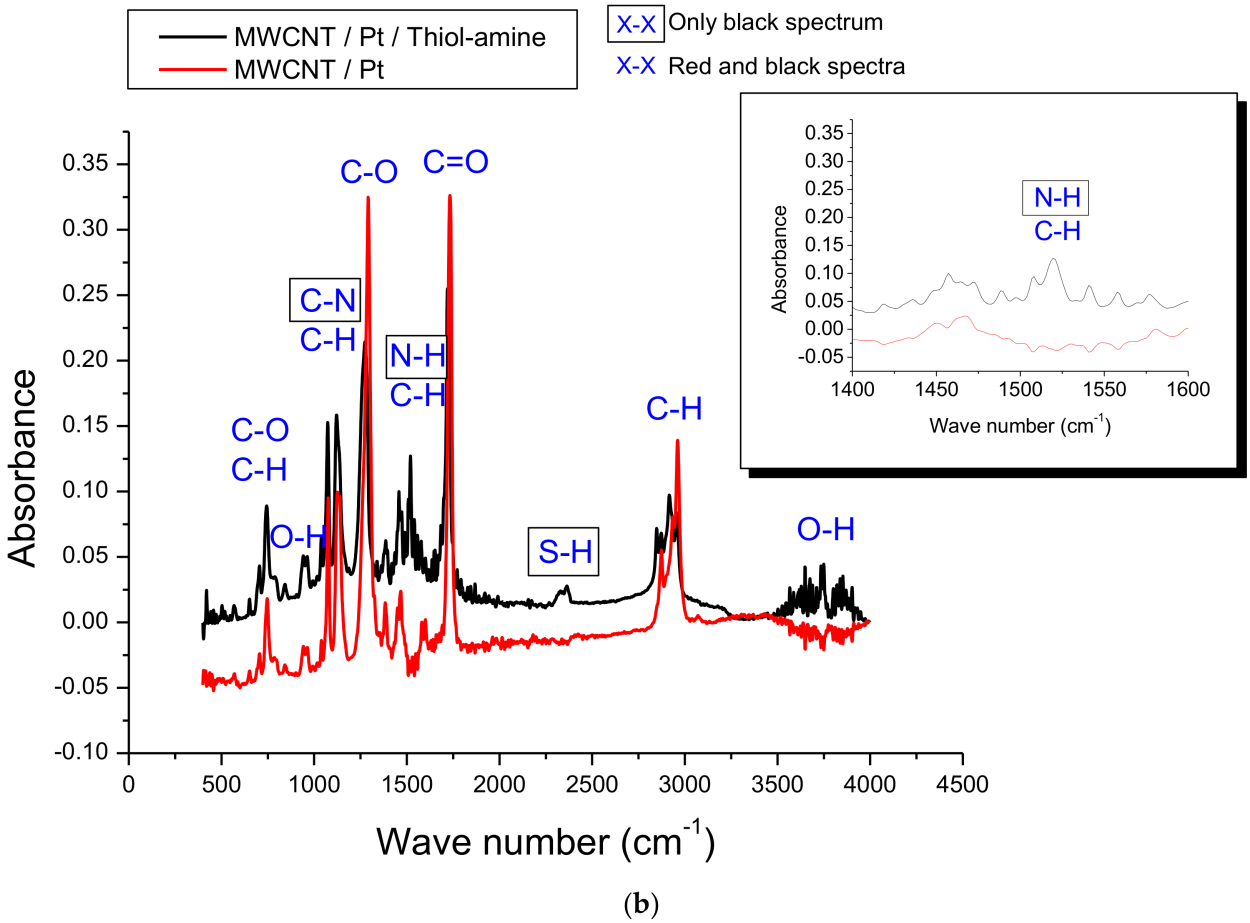

(**b**)

Figure 5. Infrared spectra of (**a**) MWCNTs/Pd and (**b**) MWCNTs/Pd/Thiol-amine films. The insets show a close view of the spectra for the N-H/C-H peaks.

The FTIR analyses show five bands in both spectra, whose wavenumbers are 3745, 2910, 1720, 1508, and 1286 cm^{-1}. According to the vibration modes, these values are attributed to O-H elongation, C-H elongation, C=O elongation, C-H deformation, and C-O elongation, respectively [48,71]. Moreover, the absorption bands between 663 cm^{-1} and 811 cm^{-1} (Figure 5a) and between 650 cm^{-1} and 814 cm^{-1} (Figure 5b), correspond to the chemical bonds C-H and C-O, respectively. Therefore, the analysis of these bands confirms the presence of the oxygenated vacant positions and functional groups grafted on the surface of MWCNTs [72]. The appearance of two bands (2800–3000 cm^{-1}) in both figures is due to the presence of C-H groups in the alkyl chain of the thiol-amine monolayer, and to the CH (sp2) hybridization groups present in the MWCNTs [73].

The two peaks located, respectively, at 1515 cm^{-1} and 1106 cm^{-1} in Figure 5a and similarly at 1510 cm^{-1} and 1098 cm^{-1} in Figure 5b (this area is enlarged in the insets) are attributed to the chemical bonds N-H and C-N. This confirms the nature of the SAM layer achieved during the functionalization of Pd and Pt loaded MWCNTs.

Finally, another band appears centred at 2344 cm^{-1} (Figure 5a) and at 2350 cm^{-1} (Figure 5b) only in the MWCNTs/Pd/Thiol-amine and MWCNTs/Pt/Thiol-amine. This band corresponds to the vibration mode of the S-H bond [73,74]. This indicates that a small amount of thiol-amine chains remains unbound to the nanoparticles even after the cleaning procedure. Indeed, the results of FTIR confirm the covalent functionalization of MWCNTs/Pd and MWCNTs/Pt by thiol-amine monolayers.

3.2. Detection of Volatile Organic Compounds (VOCs)

The sensing performances at room temperature of the four nanocomposites developed were assessed towards the VOCs gases susceptible to be biomarkers of several diseases in exhaled breath. Specifically, three of these molecules (ethanol, methanol, and benzene) were tested in the 1–13 ppm range, while toluene detection was evaluated from 0.5 to 8.5 ppm.

Figures 6 and 7 show the responses of the MWCNTs/Pd and MWCNTs/Pt sensors, respectively. It is well-known that carbon nanotube mats behave as mild p-type semiconductors, therefore, the interaction with reducing gases such as the VOCs detected here, results in an increase in their resistance. Despite the fact that the adsorption of these vapours on the metal-decorated MWCNTs films leads to a reduction in the electrical conductivity of the sensor, the dynamic responses show weak interactions between the vapour molecules and the sensitive films. On the one hand, the exposure to VOCs vapours induces slight resistance chances, revealing a limited interaction and thus, a poor energy transfer between the electron-donor molecules and the metal decorated carbon nanotubes. On the other hand, relatively fast recovery of the baseline after the gas injection is observed. This weak interaction can be explained by the appearance of a phenomenon of physisorption between the sensitive layer and the target vapours. Nevertheless, comparing the sensing performance towards the four VOCs tested, it appears that methanol detection is the most stable since lower baseline drift is experienced. This is true both for Pd and Pt decorated MWCNT sensors.

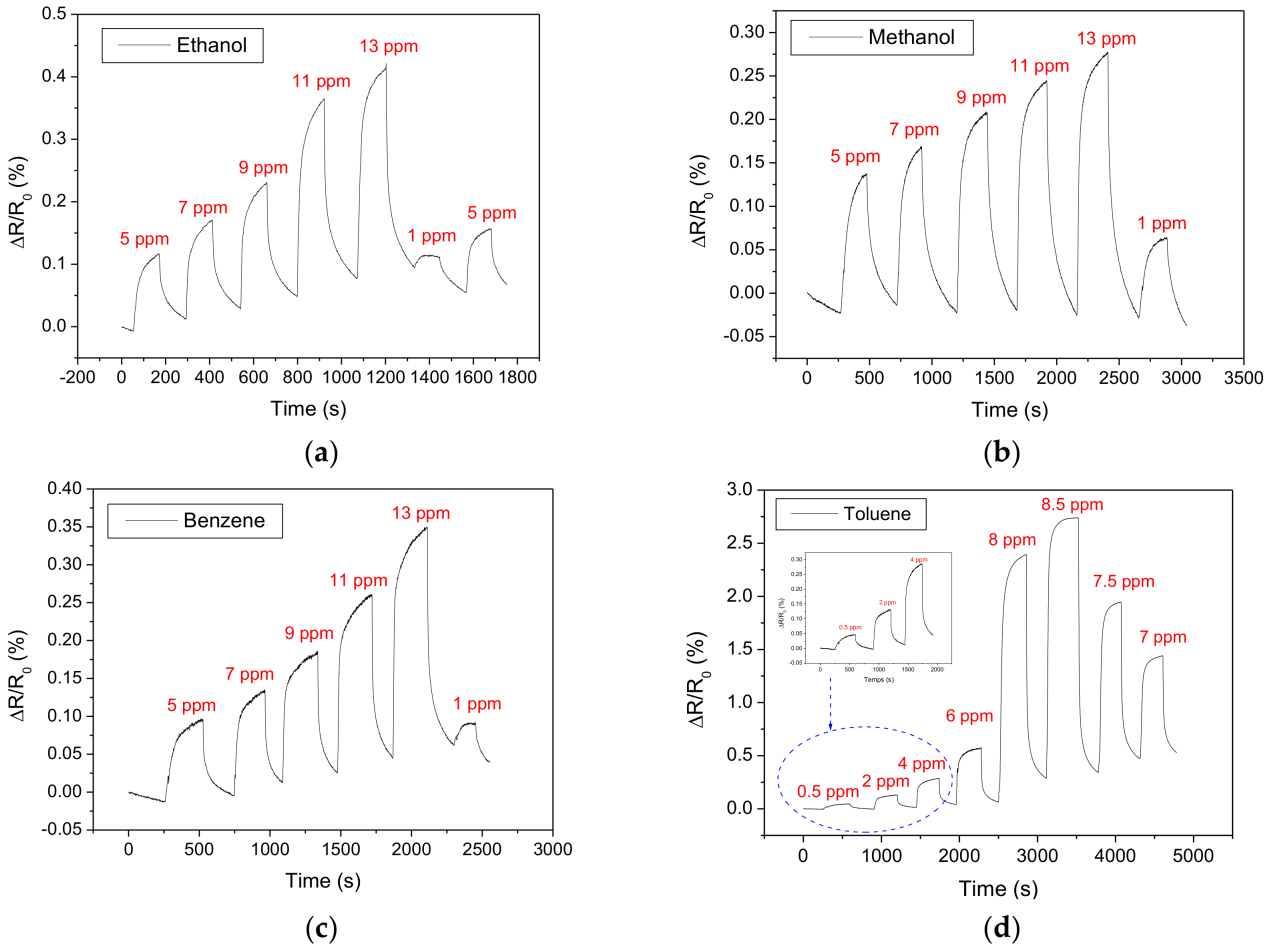

Figure 6. MWCNT/Pd sensor responses for different concentrations of the injected vapours of (**a**) ethanol, (**b**) methanol, (**c**) benzene, (**d**) toluene.

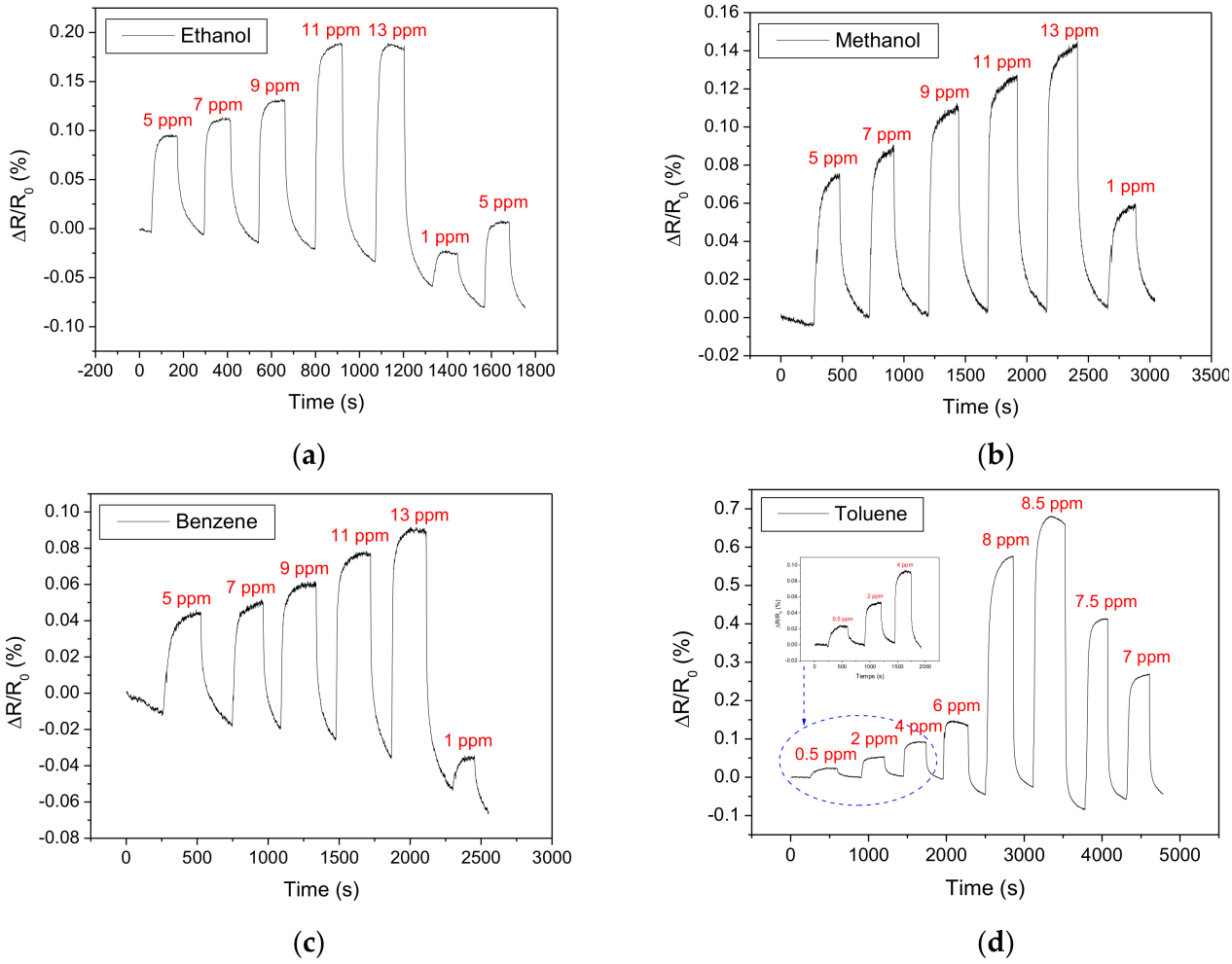

Figure 7. MWCNT/Pt sensor responses for different concentrations of the injected vapours of (**a**) ethanol, (**b**) methanol, (**c**) benzene, (**d**) toluene.

Similarly, Pd and Pt decorated MWCNTs functionalised with thiol-amine were tested under the same experimental conditions than those applied for MWCNTs decorated with Pd and Pt nanoparticles only.

Figures 8 and 9 show the results obtained for VOCs detection by using MWCNTs/Pd/Thiol-amine and MWCNTs/Pt/Thiol-amine sensors, respectively. Comparing the thiol-amine functionalized sensors with their bare metal decorated CNTs counterparts, it can be observed that Pd decorated and thiol-amine functionalised MWCNTs show significantly higher sensing responses (Figure 8), especially for toluene vapours.

Conversely, MWCNTs/Pt/Thiol-amine (Figure 9) show changes in the electrical conductivity that are only slightly higher than those registered for the bare metal decorated nanotubes. In addition, these signals are noisier in MWCNTs/Pt/Thiol-amine sensors. Considering the fast and straightforward baseline recovery for all vapours detected, it can be assumed that there is a low energy interaction between the vapour molecules and sensitive films, even when they are functionalized with thiol-amines. These weak interactions can be explained by the appearance physisorption between the sensitive layer of the sensors functionalized by a monolayer of the thiol-amine and the molecules of the vapours to be detected. Therefore, the interactions registered here could involve electrostatic interactions such as hydrogen bonds, resulting in a weak energy binding between the gas molecules and the sensor surface.

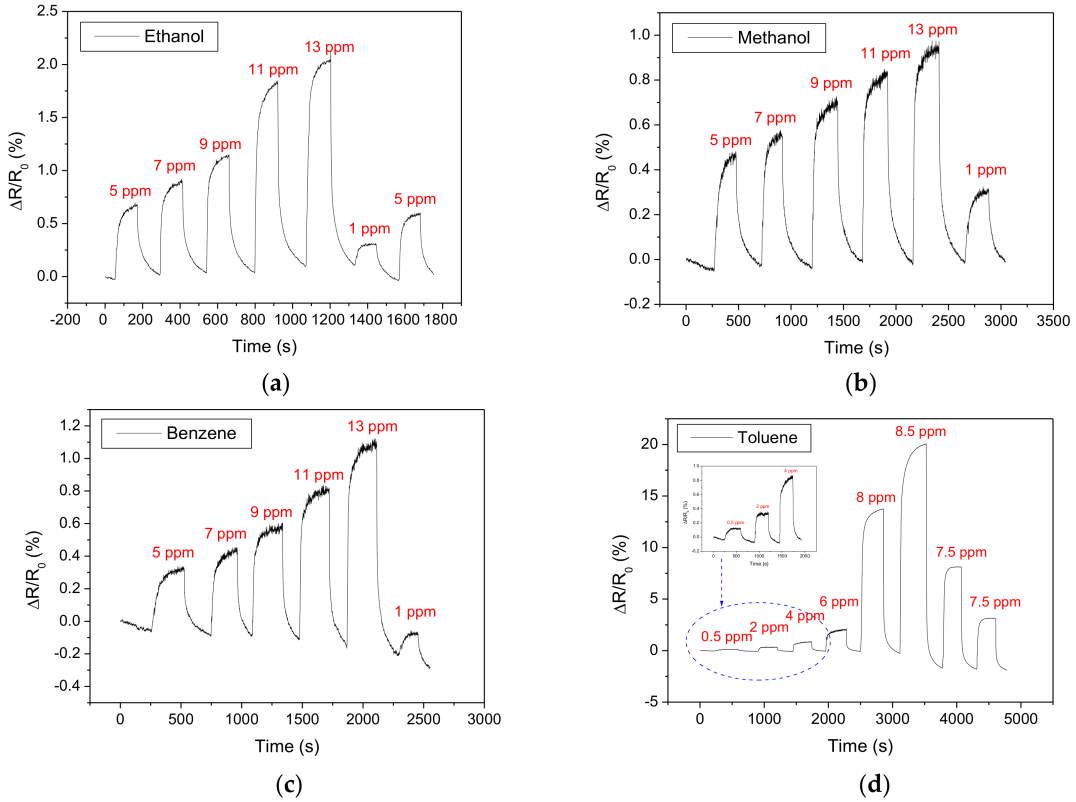

Figure 8. MWCNT/Pd/Thiol-amine sensor responses for different concentrations of the injected vapours of (**a**) ethanol, (**b**) methanol, (**c**) benzene, (**d**) toluene.

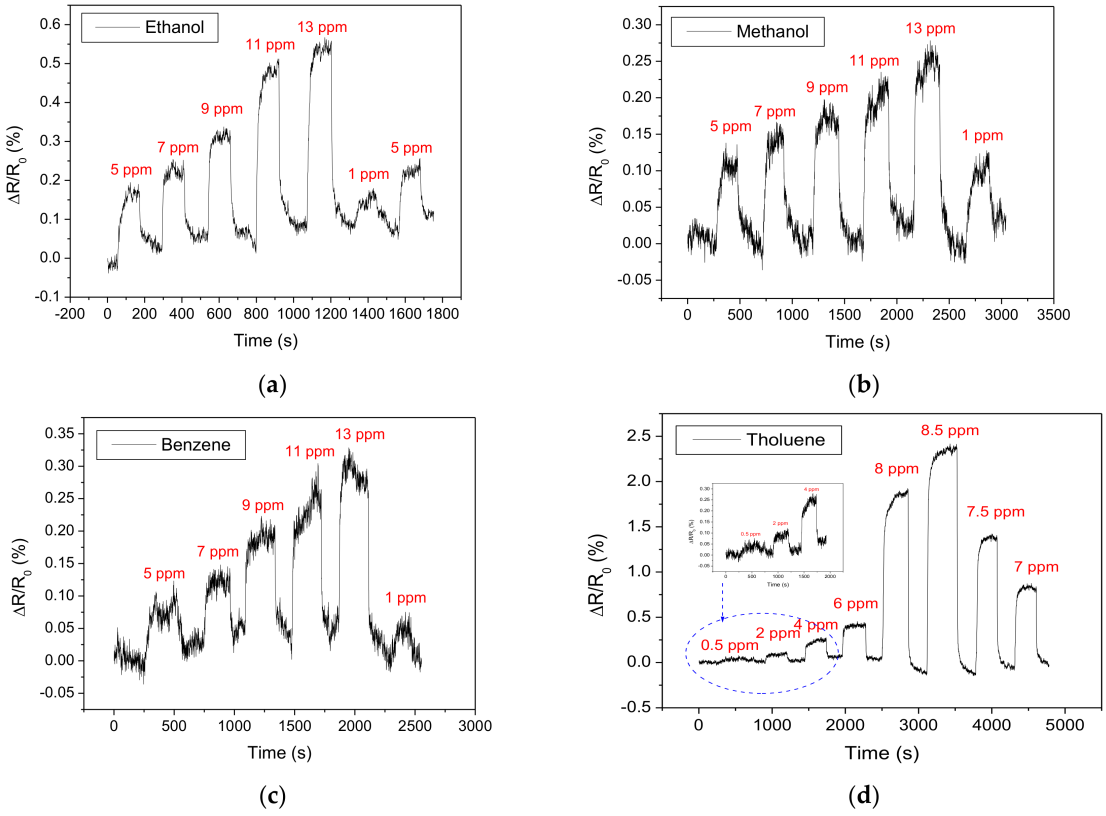

Figure 9. MWCNT/Pt/Thiol-amine sensor responses for different concentrations of the injected vapours of (**a**) ethanol, (**b**) methanol, (**c**) benzene, (**d**) toluene.

The different sensors tested show good dynamic characteristics. Thiol-amine functionalised sensors show slightly faster response dynamics in comparison to Pt or Pd loaded MWCNT sensors. Tables 2 and 3 combine the response time measurements (rise time and fall time in seconds) for each sensor for the detection of aromatic and non-aromatic VOCs. Response and recovery times are defined as the time needed for reaching 90% of the maximum response value during an exposure and the time needed for reaching 10% of the maximum response value during a baseline recovery, respectively. The average values were calculated (together with standard errors) over the response and recovery times for the different concentrations tested over five replicate measurement cycles. These values of a few ten seconds are often observed for room-temperature operated sensors employing mats of carbon nanotubes [23,28,30,31,36,46]. While the sensors show clearly that they can regain their baseline at room temperature (no baseline correction has been implemented for the sensor responses shown in any of the figures above), it can be seen as well that some baseline instability and drift exists. This drift is more evident when a small concentration of a target vapour is measured after having recovered from an exposure to a high concentration. In a practical application, this issue could be addressed by applying mild heating regularly to the sensors (i.e., introducing a short heating period to promote a more effective cleaning of the sensor surface and then sensing again at room temperature) or by applying a baseline correction algorithm.

Table 2. The response time values (in seconds) for each sensor for the detection of aromatic and non-aromatic VOCs.

Values Time (s)	Ethanol	Methanol	Benzene	Toluene
MWCNTs/Pd	41 ± 4	64 ± 5	77 ± 5	42 ± 4
MWCNTs/Pd/Thiol-amine	29 ± 3	64 ± 5	67 ± 5	36 ± 4
MWCNTs/Pt	22 ± 3	64 ± 5	52 ± 4	42 ± 4
MWCNTs/Pt/Thiol-amine	15 ± 2	62 ± 5	58 ± 4	40 ± 4

Table 3. The recovery time values (in seconds) for each sensor for the detection of aromatic and non-aromatic VOCs.

Values Time (s)	Ethanol	Methanol	Benzene	Toluene
MWCNTs/Pd	129 ± 10	294 ± 12	223 ± 11	162 ± 10
MWCNTs/Pd/Thiol-amine	122 ± 10	281 ± 12	123 ± 10	127 ± 10
MWCNTs/Pt	118 ± 10	269 ± 12	129 ± 10	183 ± 11
MWCNTs/Pt/Thiol-amine	71 ± 8	192 ± 11	83 ± 7	123 ± 10

3.3. Comparative Analysis

Figure 10 summarizes the calibration curves obtained for the four sensitive layers developed towards the different VOCs tested. The calibration curves were obtained via a statistic study on the same sample for each configuration using five replicate measurement cycles. Comparing the bare metal decorated carbon nanotubes, enhanced sensing performance was revealed when the nanotubes are decorated with palladium instead of platinum nanoparticles. Indeed, MWCNTs/Pd show higher resistance changes towards the four VOCs injected, revealing an overall improvement when it is compared with the MWCNTs/Pt sample.

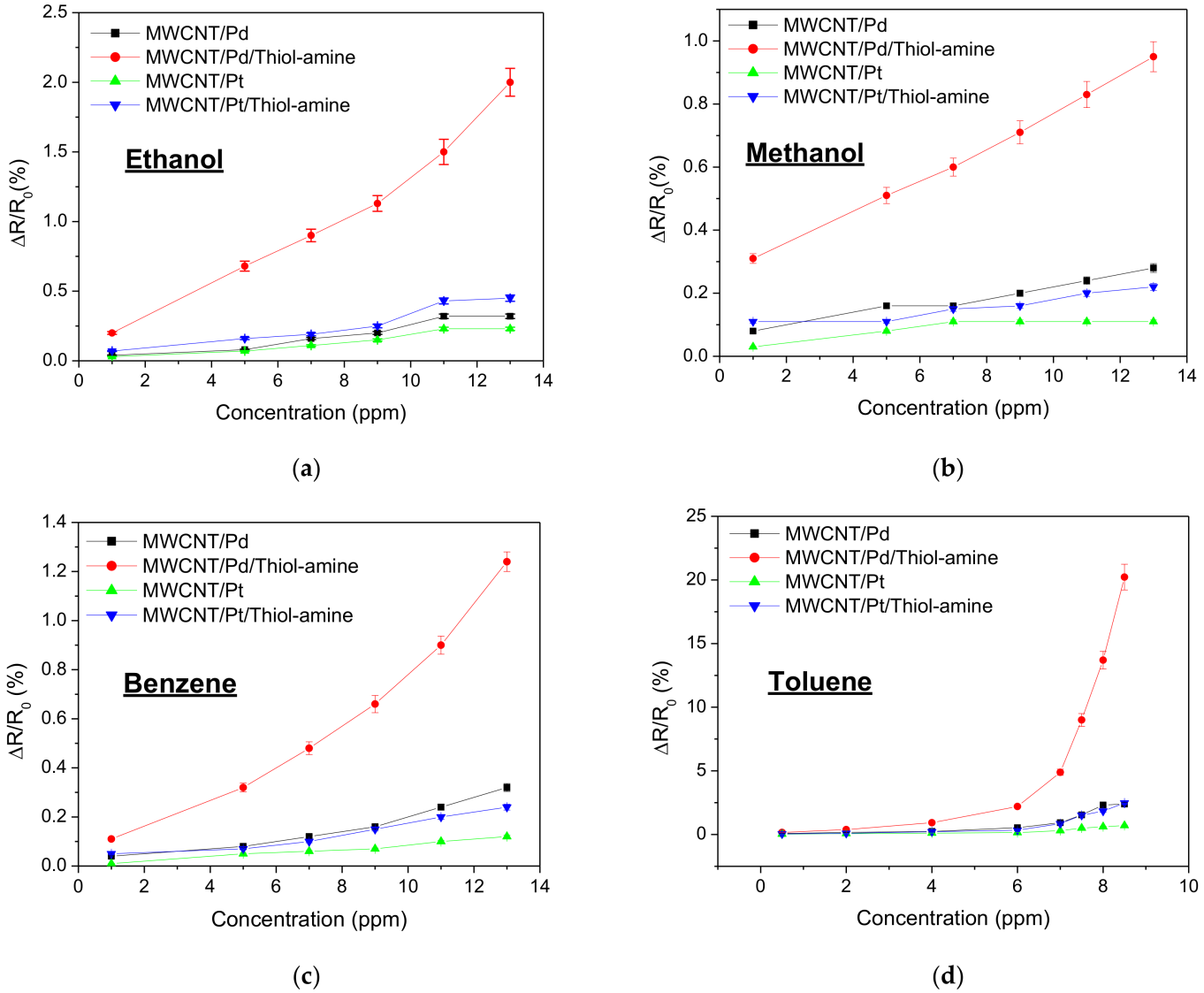

Figure 10. Calibration curves of the MWCNTs/Pd, MWCNTs/Pt, MWCNTs/Pd/Thiol-amine and MWCNTs/Pt/Thiol-amine sensors for different concentrations of injected vapours of (**a**) ethanol and (**b**) methanol and (**c**) benzene and (**d**) toluene.

Besides, Figure 10 includes the calibration curves registered for the gas sensors decorated by metallic nanoparticles and functionalized by the thiol-amine monolayer. Specifically, MWCNT decorated with platinum nanoparticles show slightly higher responses when they are functionalized by the thiol-amine monolayer. Nevertheless, it is worth noting that MWCNT/Pd/Thiol-amine sensors show greater sensor responses to the four VOCs tested than the other sensitive films. In particular, MWCNT/Pd/Thiol-amine shows higher resistance changes (up to 4-fold) to ethanol, methanol and benzene than their Pt counterpart. For toluene, a 10-fold increase in response is observed for the MWCNTs/Pd/Thiol-amine sensor. In fact, this sensor is about 15 times more responsive to toluene than to any other VOC tested, which confers some selectivity towards this aromatic VOC.

4. Discussion

The detection results achieved at room temperature (especially the good recovery) support the physisorption of the different vapour molecules tested on the sensor surface. Indeed, the gas molecule adsorption on the films of our sensors leads to a considerable increase in resistivity in all cases. This phenomenon is due to the nature of the injected

vapours, which behave as reducing gases. In fact, carbon nanotubes are well-known *p*-type semiconductors, and in consequence, the adsorption of the reducing vapour molecules leads to a decrease in the majority carriers (holes) in the sensitive film. As a result, when the sensors are exposed to these electron-donor VOCs molecules, a decrease in the conductivity is induced, which translates into an increase in the electrical resistance measured. Besides, according to Hiroki et al., the work function of oxygen-treated MWCNT varies from 4.9 to 5.1 eV [75]; these values are very close to those of metals such as Pt, which is 4.8 eV and Pd, which is 4.95 eV [49]. This facilitates the movement of electrons between metallic nanoparticles and MWCNTs, with the direction of charge transfer as a function of the gaseous environment. Indeed, the electronegativity values of Pt and Pd are very similar, and therefore the weight is relative as a percentage of the metallic dopants in the sensors.

Comparing the sensing performance of bare metal NP decorated MWCNTs in Figure 10, it can be appreciated that there are higher responses when the carbon nanotubes are decorated with palladium NPs rather than platinum. Since the interaction between both metal nanoparticles and the different VOCs tested cannot be completely ruled out, no significant interactions can be expected. This is due to the room temperature working conditions because it is well-known that metal nanoparticles need higher temperatures to activate their catalytic properties. Additionally, both nanoparticles almost show the same size distribution. Therefore, the differences that appear in their responses are probably derived from the sputtering decoration conditions. This means that the power and plasma exposure time used for the decoration of MWCNT/Pt was significantly higher than those used for the MWCNT/Pd sensor. In consequence, this may lead to a more defective surface for the sensor decorated by the Pt and lead to a degradation of the electronic properties of the MWCNTs. This could explain the higher levels of noise experienced with MWCNT/Pt and MWCNT/Pt/Thiol-amine sensors.

Regarding the results obtained with thiol-amine functionalized carbon nanotubes, they always show better sensing responses than the bare metal NP decorated nanotubes. The reason could be explained by the concentration of surface species able to interact with the gases. In other words, metal NPs decorated MWCNTs show low sensitivities due to the limited interaction between gases and few oxygen functional groups grafted at the walls of the nanotubes. However, once the decorated nanotubes are functionalized with thiols, there is a large increment in the available species able to interact with the gases. In particular, amine functional groups can act as recognition elements; meanwhile, nanotubes will act as transducers.

However, it is interesting to point out that thiol-functionalized nanotubes with Pd nanoparticles show significantly higher sensitivities than those decorated with Pt. According to Figure 5, the relative intensity of the N-H peak is higher in MWCNT/Pd/Thiol-amine than in MWCNT/Pt/Thiol amine samples. This probably indicates a higher concentration of thiol-amines functionalizing Pd than Pt. Thus, this can explain the higher sensitivities registered when nanotubes are decorated with Pd, due to the larger concentration of recognition elements (thiols). In other words, a large number of amine groups are able to interact with the gas molecules. Then, MWCNT/Pt/Thiol-amine show slightly enhanced responses compared to the nanotubes decorated only with platinum due to the lower presence of thiols. Nevertheless, some reasons should be beyond the poor thiol functionalization of Pt nanoparticles in comparison to the more effective functionalization of Pd NPs. There are two main reasons to explain this. The first one is related to the nanoparticle size, due to Pd nanoparticles presenting slightly higher diameters. In consequence, Pd NPs lead to a higher and more efficient thiol-functionalization due to their large surface area to volume ratio. The second reason could be based on the interaction between thiol-amine groups and metallic nanoparticles. Some works report the opposite behaviour between thiol and amine groups regarding the Pt NP size [76]. This means that higher Pt size induces a higher thiol binding, whereas an opposite trend is observed for amine groups. This means that the reduced diameter of the Pt NPs used could promote the binding with amine groups instead of the thiols. Therefore, if amine groups interact with Pt NPs, a reduced number of

functional groups are available to interact with gases. Conversely, small Pd NPs have been demonstrated as a great nanomaterial to be functionalized with thiols [77]. Additionally, apart from this better thiol functionalization of palladium nanoparticles, the work function of Pd is better aligned to the one of carbon nanotubes than the one of Pt. Therefore, the sensing layer with Pd NPs will lead to a more efficient charge transfer, enhancing the sensing performance even more.

In addition, the superior response of the MWCNTs/Pd/Thiol-amine sensor to the different vapours (and, particularly, toluene) is directly related to the self-assembled monolayers used. Indeed, the monolayers which have a hydrophobic functional group, such as -NH2 and long carbon chains (11 carbon atoms in our case), show improved sensitivity to all the vapours tested, as the amine group can act as donor or acceptor in hydrogen bond formation. This could explain why there is a significant improvement in the response achieved for all the volatiles tested. The higher improvement in responsiveness and selectivity achieved for toluene could be due to the higher performance of Pd NPs (as compared to Pt NPs) for the adsorption and catalytic oxidation of toluene [78], but this deserves further research. Breath samples contain high levels of moisture. While breath samples can be treated to remove moisture, the complete removal of moisture is not desirable, as this process can alter volatile composition within a breath sample. The functionalization of MWCNTs with SAMs of highly hydrophobic thiols, such as the one employed here, has been found to result in a gas-sensitive material highly resilient to ambient moisture. Casanova and co-workers reported in [79] that the gas sensing properties of MWCNT mats functionalized with hydrophobic thiols via the SAM technique were barely affected by strong humidity changes. Therefore, we can expect the results discussed here to remain valid under conditions similar to the ones of a real breath sample analysis.

5. Conclusions

The use of a self-assembled monolayer has been proved as an effective technique to grow ultrafine films over multi-walled carbon nanotubes decorated with metal nanoparticles. The reactive sulfur moiety is an excellent fixing group on the metal surface and the 11-amino-1-undecanethiol (Thiol-amine) SAM provides a convenient means of increasing the gas sensitivity of plasma treated carbon nanotubes. Besides, this functionalization opens up a straightforward strategy for increasing the reactivity of carbon nanotubes, since the length of the separation chain and/or the hydrophilic or hydrophobic nature of the terminal group of the molecule become parameters for increasing the sensitivity and the selectivity of the gas sensors. The results shown and discussed here indicate that the nanocomposites developed show potential for detecting biomarkers that appear at trace levels in exhaled breath samples, thus paving the way to their incorporation in gas sensor arrays for the analysis of complex volatile matrices in human breath applications. While our previous results indicate that moisture would not affect significantly the performance of MWCNTs functionalised with SAMs of highly hydrophobic thiols, the results are still somewhat preliminary as some major challenges are still an issue. For example, the selective detection of specific compounds (breath samples consist of a very complex mixture of volatiles) would require assessing sensor performance with volatile mixtures. In addition, while the sensors show enough responsiveness for detecting the non-aromatic biomarkers associated to NASH, the response towards aromatics should be enhanced further (e.g., by increasing the homogeneity and coverage of the SAMs on MWCNT mates). Finally, the unequivocal association of a certain compound with a certain disease or health disorder is still the subject of debate. For all these reasons, more research efforts are needed in the coming years to develop reliable, inexpensive, non-invasive, and portable sensing devices for biomarkers assessment.

Author Contributions: Conceptualization, J.C.-C. and E.L.; data curation, A.T. and M.B.M.; formal analysis, H.B.; funding acquisition, E.L. and A.A.; investigation, A.T., H.B. and M.B.M.; methodology, J.C.-C. and E.L.; supervision, J.C.-C., E.L. and A.A.; visualization, M.B.M.; writing—original draft,

A.T. and H.B.; writing—review and editing, J.C.-C., E.L. and A.A. All authors have read and agreed to the published version of the manuscript.

Funding: This work is funded by the Science for Peace and Security Program of the North Atlantic Treaty Organization (SPS-NATO) under grant no. SFP 984511 and SPS G5571. E.L. is supported by the Catalan Institution for Research and Advanced Studies via the 2018 Edition of the ICREA Academia Award. This work was funded in part by MICINN and FEDER via grant no. RTI2018-101580-B-I100 and by AGAUR under grant no. 2017 SGR 418.

Institutional Review Board Statement: Not applicable.

Informed Consent Statement: Not applicable.

Data Availability Statement: Data can be obtained from the authors upon request.

Acknowledgments: The authors thank the Alexander von Humboldt Foundation (Bonn, Germany) for the material donation.

Conflicts of Interest: The authors declare no conflict of interest.

References

1. Cikach, S.F., Jr.; Dweikab, A.R. Cardiovascular Biomarkers in Exhaled Breath. *Prog. Cardiovasc. Dis.* **2012**, *55*, 34–43. [CrossRef] [PubMed]
2. Umeno, A.; Biju, V.; Yoshida, Y. In vivo ROS production and use of oxidative stress-derived biomarkers to detect the onset of diseases such as Alzheimer's disease, Parkinson's disease, and diabetes. *Free Radic. Res.* **2017**, *51*, 413–427. [CrossRef]
3. Pauling, L.; Robinson, A.B.; Teranish, R.; Cary, P. Quantitative analysis of urine vapor and breath by gas-liquid partition chromatography. *Proc. Nat. Acad. Sci. USA* **1971**, *68*, 2374. [CrossRef]
4. Gordon, S.M.; Szidon, J.P.; Krotoszynski, B.K.; Gibbons, R.D.; O'Neill, H.J. Volatile organic compounds in exhaled air from patients with lung cancer. *Clin. Chem.* **1985**, *31*, 1278–1282. [CrossRef] [PubMed]
5. Phillips, M.; Cataneo, R.N.; Cummin, A.R.; Gagliardi, A.J.; Gleeson, K.; Greenberg, J.; Maxfield, R.A.; Rom, W.N. Detection of lung cancer with volatile markers in the breath. *Chest* **2003**, *123*, 2115–2123. [CrossRef] [PubMed]
6. Ligor, M.; Ligor, T.; Bajtarevic, A.; Ager, C.; Pienz, M.; Klieber, M.; Denz, H.; Fiegl, M.; Hilbe, W.; Weiss, W.; et al. Determination of volatile organic compounds in exhaled breath of patients with lung cancer using solid phase microextraction and gas chromatography mass spectrometry. *Clin. Chem. Lab. Med.* **2009**, *47*, 550–560. [CrossRef] [PubMed]
7. Bantz, K.C.; Meyer, A.F.; Wittenberg, N.J.; Im, H.; Kurtuluş, Ö.; Lee, S.H.; Lindquist, N.C.; Oh, S.H.; Haynes, C.L. Recent progress in SERS biosensing. *Phys. Chem. Chem. Phys.* **2011**, *13*, 11551–11567. [CrossRef]
8. Dinish, U.S.; Balasundaram, G.; Chang, Y.T.; Olivo, M. Sensitive multiplex detection of serological liver cancer biomarkers using SERS-active photonic crystal fiber probe. *J. Biophotonics* **2014**, *7*, 956–965. [CrossRef] [PubMed]
9. Vincentis, A.D.; Pennazza, G.; Santonico, M.; Gentilucci, U.V.; Galati, G.; Gallo, P.; Vernile, C.; Pedone, C.; Incalzi, R.A.; Picardi, A. Breath-print analysis by e-nose for classifying and monitoring chronic liver disease: A proof-of-concept study. *Sci. Rep.* **2016**, *6*, 25337. [CrossRef] [PubMed]
10. Nakhleh, M.K.; Amal, H.; Jeries, R. Diagnosis and Classification of 17 Diseases from 1404 Subjects via Pattern Analysis of Exhaled Molecules. *ACS Nano* **2017**, *11*, 112–125. [CrossRef] [PubMed]
11. Zhang, Y.; Gao, G.; Liu, H.; Fu, H.; Fan, J.; Wang, K.; Chen, Y.; Li, B.; Zhang, C.; Zhi, X.; et al. Identification of Volatile Biomarkers of Gastric Cancer Cells and Ultrasensitive Electrochemical Detection based on Sensing Interface of Au-Ag Alloy coated MWCNTs. *Theranostics* **2014**, *4*, 154–162. [CrossRef]
12. Giannoukos, S.; Brkić, B.; Taylor, S.; Marshall, A.; Verbeck, G.F. Chemical Sniffing Instrumentation for Security Applications. *Chem. Rev.* **2016**, *116*, 8146–8172. [CrossRef] [PubMed]
13. Gliszczyńska-Świgło, A.; Chmielewski, J. Electronic nose as a tool for monitoring the authenticity of food. A review. *Food Anal. Methods* **2017**, *10*, 1800–1816. [CrossRef]
14. Wojnowski, W.; Dymerski, T.; Gębicki, J.; Namieśnik, J. Electronic Noses in Medical Diagnostics. *Curr. Med. Chem.* **2019**, *26*, 197–215. [CrossRef] [PubMed]
15. D'Amico, A.; Pennazza, G.; Santonico, M.; Martinelli, E.; Roscioni, C.; Galluccio, G.; Paolesse, R.; Natale, C.D. An investigation on electronic nose diagnosis of lung cancer. *Lung Cancer* **2010**, *68*, 170–176. [CrossRef] [PubMed]
16. Chang, J.E.; Lee, D.S.; Ban, S.W.; Oh, J.; Jung, M.Y.; Kim, S.H.; Park, S.J.; Persaud, K.; Jheon, S. Analysis of volatile organic compounds in exhaled breath for lung cancer diagnosis using a sensor system. *Sens. Actuators B Chem.* **2018**, *255*, 800–807. [CrossRef]
17. Dymerski, T.; Gębicki, J.; Wiśniewska, P.; Sliwińska, M.; Wardencki, W.; Namieśnik, J. Application of the electronic nose technique to differentiation between model mixtures with COPD markers. *Sensors* **2013**, *13*, 5008–5027. [CrossRef]
18. Bannier, M.A.G.E.; van de Kant, K.D.G.; Jöbsis, Q.; Dompeling, E. Feasibility and diagnostic accuracy of an electronic nose in children with asthma and cystic fibrosis. *J. Breath Res.* **2019**, *13*, 1752–7163. [CrossRef]

19. Roine, A.; Veskimäe, E.; Tuokko, A.; Kumpulainen, P.; Koskimäki, J.; Keinänen, T.A.; Häkkinen, M.R.; Vepsäläinen, J.; Paavonen, T.; Lekkala, J.; et al. Detection of Prostate Cancer by an Electronic Nose: A Proof of Principle Study. *Am. Urol. Assoc. J.* **2014**, *192*, 230–235. [CrossRef]
20. Covington, J.A.; Westenbrink, E.W.; Ouaret, N.; Harbord, R.; Bailey, C.; O'Connell, N.; Cullis, J.; Williams, N.; Nwokolo, C.U.; Bardhan, K.D.; et al. Application of a novel tool for diagnosing bile acid diarrhea. *Sensors* **2013**, *13*, 11899–11912. [CrossRef] [PubMed]
21. Iijima, S. Helical microtubules of graphitic carbon. *Nature* **1991**, *354*, 56–58. [CrossRef]
22. Li, J.; Lu, Y.; Meyyappan, M. Nano Chemical Sensors with Polymer-Coated Carbon Nanotubes. *IEEE Sens. J.* **2006**, *6*, 1047–1051. [CrossRef]
23. Lu, Y.; Li, J.; Han, J.; Ng, H.-T.; Binder, C.; Partridge, C.; Meyyappan, M. Room temperature methane detection using palladium loaded single-walled carbon nanotube sensors. *Chem. Phys. Lett.* **2004**, *391*, 344–348. [CrossRef]
24. Mubeen, S.; Zhang, T.; Yoo, B.; Deshusses, M.A.; Myung, N.V.J. Palladium Nanoparticles Decorated Single-Walled Carbon Nanotube Hydrogen Sensor. *Phys. Chem. C* **2007**, *111*, 6321–6327. [CrossRef]
25. Consales, M.; Campopiano, S.; Cutolo, A.; Penza, M.; Aversa, P.; Cassano, G.; Giordano, M.; Cusano, A. Carbon nanotubes thin films fiber optic and acoustic VOCs sensors: Performances analysis. *Sens. Actuators B* **2006**, *118*, 232–242. [CrossRef]
26. Ryota, Y.; Kiyohiko, T.; Toshinari, I.; Tetsuya, O.; Yasushi, A.; Takashi, M. Characterization and field emission properties of multi-walled carbon nanotubes with fine crystallinity prepared by CO_2 laser ablation. *Appl. Surf. Sci.* **2012**, *258*, 6958–6962.
27. Kuberský, P.; Sedlák, P.; Hamáček, A.; Nešpůrek, S.; Kuparowitz, T.; Šikula, J.; Majzner, J.; Sedlaková, V.; Grmela, L.; Syrový, T. Quantitative fluctuation-enhanced sensing in amperometric NO_2 sensors. *Chem. Phys.* **2015**, *456*, 111–117. [CrossRef]
28. Villalpando-Páez, F.; Romero, A.H.; Muñoz-Sandoval, E.; Martınez, L.M.; Terrones, H.; Terrones, M. Fabrication of vapor and gas sensors using films of aligned CNx nanotubes. *Chem. Phys. Lett.* **2004**, *386*, 137–143. [CrossRef]
29. Bai, L.; Zhou, Z. Computational study of B- or N-doped single-walled carbon nanotubes as NH_3 and NO_2 sensors. *Carbon* **2007**, *45*, 2105–2110. [CrossRef]
30. Adjizian, J.J.; Leghrib, R.; Koos, A.A.; Suarez-Martinez, I.; Crossley, A.; Wagner, P.; Grobert, N.; Llobet, E.; Ewels, C.P. Boron- and nitrogen-doped multi-wall carbon nanotubes for gas detection. *Carbon* **2014**, *66*, 662–673. [CrossRef]
31. Ionescu, R.; Espinosa, E.H.; Sotter, E.; Llobet, E.; Vilanova, X.; Correig, X.; Felten, A.; Bittencourt, C.; van Lier, G.; Charlier, J.-C.; et al. Oxygen functionalisation of MWNT and their use as gas sensitive thick-film layers. *Sens. Actuators B Chem.* **2006**, *113*, 36–46. [CrossRef]
32. Saito, T.; Matsushige, K.; Tanaka, K. Chemical treatment and modification of multi-walled carbon nanotubes. *Phys. B Condens. Matter* **2002**, *323*, 280–283. [CrossRef]
33. Charlier, J.C.; Arnaud, L.; Avilov, I.V.; Delgado, M.; Demoisson, F.; Espinosa, E.H.; Ewels, C.P.; Felten, A.; Guillot, J.; Ionescu, R.; et al. Carbon nanotubes randomly decorated with gold clusters: From nano-hybrid atomic structures to gas sensing prototypes. *Nanotechnology* **2009**, *20*, 375501. [CrossRef] [PubMed]
34. Wei, B.-Y.; Hsu, M.-C.; Su, P.-G.; Lin, H.-M.; Wu, R.-J.; Lai, H.-J. A novel SnO_2 gas sensor doped with carbon nanotubes operating at room temperature. *Sens. Actuators B Chem.* **2004**, *101*, 81–89. [CrossRef]
35. Bittencourt, C.; Felten, A.; Espinosa, E.H.; Ionescu, R.; Llobet, E.; Correig, X.; Pireaux, J.-J. WO_3 films modified with functionalised multi-wall carbon nanotubes: Morphological, compositional and gas response studies. *Sens. Actuators B Chem.* **2006**, *115*, 33–41. [CrossRef]
36. de Luca, L.; Donato, A.; Santangelo, S.; Faggio, G.; Messina, G.; Donato, N.; Neri, G. Hydrogen sensing characteristics of Pt/TiO2/MWCNTs composites. *Int. J. Hydrog. Energ.* **2012**, *37*, 1842–1851. [CrossRef]
37. Trocino, S.; Donato, A.; Latino, M.; Donato, N.; Leonardi, S.G.; Neri, G. Pt- TiO_2/MWCNTs Hybrid composites for monitoring low hydrogen concentrations in air. *Sensors* **2012**, *12*, 12361–12373. [CrossRef]
38. Clément, P.; Hafaiedh, I.; Parra, E.J.; Thamri, A.; Guillot, J.; Abdelghani, A.; Llobet, E. Iron oxide and oxygen plasma functionalized multi-walled carbon nanotubes for the discrimination of volatile organic compounds. *Carbon* **2014**, *78*, 510–520. [CrossRef]
39. Dai, L.M.; Soundarrajan, P.; Kim, T. Sensors and sensor arrays based on conjugated polymers and carbon nanotubes. *Pure App. Chem.* **2002**, *74*, 1753–1772. [CrossRef]
40. Tsubokawa, N. Preparation and properties of polymer-grafted carbon nanotubes and nanofibers. *Polym. J.* **2005**, *37*, 637–655. [CrossRef]
41. Castro, M.; Lu, J.; Bruzaud, S.; Kumar, B.; Feller, J.-F. Carbon nanotubes/poly(ε-caprolactone) composite vapour sensors. *Carbon* **2007**, *47*, 1930–1942. [CrossRef]
42. Mengning, D.; Yifan, T.; Pingping, G.; Michael, J.R.; Alexander, S. Chemical sensing with polyaniline coated single-walled carbon nanotubes. *Adv. Mater.* **2011**, *23*, 536–540.
43. Gang, P.; Elena, T.; Hossam, H. Detecting simulated patterns of lung cancer biomarkers by random network of single-walled carbon nanotubes coated with nonpolymeric organic materials. *Nano Lett.* **2008**, *8*, 3631–3635.
44. Zilberman, Y.; Tisch, U.; Shuster, G.; Pisula, W.; Feng, X.; Müllen, K.; Haick, H. Carbon nanotube/hexa-peri-hexabenzocoronene bilayers for discrimination between nonpolar volatile organic compounds of cancer and humid atmospheres. *Adv. Mat.* **2010**, *22*, 4317–4320. [CrossRef] [PubMed]
45. Zilberman, Y.; Ionescu, R.; Feng, X.; Müllen, K.; Haick, H. Nanoarray of polycyclic aromatic hydrocarbons and carbon nanotubes for accurate and predictive detection in realworld environmental humidity. *ACS Nano* **2011**, *5*, 6743–6753. [CrossRef]

46. Baccar, H.; Thamri, A.; Clément, P.; Llobet, E.; Abdelghani, A. Pt- and Pd-decorated MWCNTs for vapour and gas detection at room temperature. *Beilstein J. Nanotechnol.* **2015**, *6*, 919–927. [CrossRef] [PubMed]
47. Thamri, A.; Baccar, H.; Clément, P.; Llobet, E.; Abdelghani, A. Rhodium-decorated MWCNTs for detecting organic vapours. *Int. J. Nanotechnol.* **2015**, *12*, 562–571. [CrossRef]
48. Thamri, A.; Baccar, H.; Struzzi, C.; Bittencourt, C.; Abdelghani, A.; Llobet, E. MHDA-Functionalized Multiwall Carbon Nanotubes for detecting non-aromatic VOCs. *Sci. Rep.* **2016**, *6*, 35130. [CrossRef]
49. Leghrib, R.; Felten, A.; Demoisson, F.; Renier, F.; Pireaux, J.J.; Llobet, E. Room-temperature, selective detection of benzene at trace levels using plasma- treated metal-decorated multiwalled carbon nanotubes. *Carbon* **2010**, *48*, 3477–3484. [CrossRef]
50. Star, A.; Joshi, V.; Skarupo, S.; Thomas, D.; Gabriel, J.C.P. Gas sensor array based on metal-decorated carbon nanotubes. *Phys. Chem.* **2006**, *110*, 21014–21020. [CrossRef] [PubMed]
51. Nasiri, A.; Shariaty-Niasar, M.; Rashidi, A.M.; Khodafarin, R. Effect of CNT structures on thermal conductivity and stability of nanofluid. *Int. J. Heat Mass Transfer* **2012**, *55*, 1529–1535. [CrossRef]
52. Mohiuddin, M.; Hoa, S.V. Temperature dependent electrical conductivity of CNT–PEEK composites, Compos. *Sci. Technol.* **2011**, *72*, 21–27.
53. Chiu, W.-C.; Tsui, B.-Y. Characteristics of size dependent conductivity of the CNT-interconnects formed by low temperature process. *Microelectron. Reliab.* **2013**, *53*, 906–911. [CrossRef]
54. El-Sayed, I.H.; Huang, X.; El-Sayed, M.A. Surface plasmon resonance scattering and absorption of anti-EGFR antibody conjugated gold nanoparticles in cancer diagnostics: Applications in oral cancer. *Nano Lett.* **2005**, *5*, 829–834. [CrossRef] [PubMed]
55. Liu, D.; Leech, H.J. Application of Colloidal Gold in Protein Immobilization, Electron Transfer, and Biosensing. *Anal. Lett.* **2003**, *36*, 1–19. [CrossRef]
56. Costello, B.L.; Amann, A.; Al-Kateb, H.; Flynn, C.; Filipiak, W.; Khalid, T.; Osborne, D.; Ratcliffe, N.M. A review of the volatiles from the healthy human body. *J. Breath Res.* **2014**, *8*, 014001. [CrossRef] [PubMed]
57. Meinardi, S.; Jin, K.B.; Barletta, B.; Blake, D.R.; Vaziri, N.D. Exhaled breath and fecal volatile organic biomarkers of chronic kidney disease. *Biochim. Biophys. Acta (BBA) Gen. Subj.* **2013**, *3*, 2531–2537. [CrossRef] [PubMed]
58. Korte, J.E.; Hertz-Picciotto, I.; Schulz, M.R.; Ball, L.M.; Duell, E.J. The contribution of benzene to smoking-induced leukemia. *Environ. Health Perspect* **2000**, *108*, 333–339.
59. Cope, K.; Risby, T.; Diehl, A.M. Increased gastrointestinal ethanol production in obese mice: Implications for fatty liver disease pathogenesis. *Gastroenterology* **2000**, *5*, 1340–1347. [CrossRef] [PubMed]
60. Španěl1, P.; Dryahina, K.; Vicherková, P.; Smith, D. Increase of methanol in exhaled breath quantified by SIFT-MS following aspartame ingestion. *J. Breath Res.* **2015**, *9*, 047104. [CrossRef]
61. Swithers, S.E. Artificial sweeteners produce the counterintuitive effect of inducing metabolic derangements. *Trends Endocrinol. Metab.* **2013**, *9*, 431–441. [CrossRef] [PubMed]
62. Koureas, M.; Kirgou, P.; Amoutzias, G.; Hadjichristodoulou, C.; Gourgoulianis, K.; Tsakalof, A. Target Analysis of Volatile Organic Compounds in Exhaled Breath for Lung Cancer Discrimination from Other Pulmonary Diseases and Healthy Persons. *Metabolites* **2020**, *10*, 317. [CrossRef] [PubMed]
63. Bajtarevic, A.; Ager, C.; Pienz, M.; Klieber, M.; Schwarz, K.; Ligor, M.; Ligor, T.; Filipiak, W.; Denz, H.; Fiegl, M.; et al. Noninvasive detection of lung cancer by analysis of exhaled breath. *BMC Cancer* **2009**, *9*, 1471–2407. [CrossRef] [PubMed]
64. Jia, Z.; Patra, A.; Kutty, V.K.; Venkatesan, T. Critical Review of Volatile Organic Compound Analysis in Breath and In Vitro Cell Culture for Detection of Lung Cancer. *Metabolites* **2019**, *9*, 52. [CrossRef]
65. Gashimova, E.; Temerdashev, A.; Porkhanov, V.; Polyakov, I.; Perunov, D.; Azaryan, A.; Dmitrieva, E. Investigation of different approaches for exhaled breath and tumor tissue analyses to identify lung cancer biomarkers. *J. Heliyon* **2020**, *6*, 2405–8440.
66. José-Yacamán, M.; Miki-Yoshida, M.; Rendon, L.; Santiesteban, J.G. Catalytic growth of carbon microtubules with fullerene structure. *Appl. Phys. Lett.* **1993**, *62*, 202–204. [CrossRef]
67. Valentini, L.; Cantalini, C.; Armentano, I.; Kenny, J.M.; Lozzi, L.; Santucci, S. Highly sensitive and selective sensors based on carbon nanotubes thin films for molecular detection. *Diam. Relat. Mater.* **2004**, *13*, 1301–1305. [CrossRef]
68. Hafaiedh, I.; Clément, P.; Baccar, H.; Llobet, E.; Abdelghani, A. Functionalized multi-walled carbon nanotubes for chemical vapour detection. *Int. J. Nanotechnol.* **2013**, *10*, 485–495. [CrossRef]
69. Techane, D.S.; Gamble, L.J.; Castner, D.G. Multi-technique characterization of self-assembled carboxylic acid terminated alkanethiol monolayers on nanoparticle and flat gold surfaces. *J. Phys. Chem. C Nanomater. Interfaces* **2011**, *115*, 9432–9441. [CrossRef] [PubMed]
70. Thamri, A.; Baccar, H.; Annanouch, F.E.; Llobet, E.; Abdelghani, A. Methanol, Ethanol and Acetone Sensing Using AACVD-grown Tungsten Oxide Nanoneedles. *J. Nanomed. Nanotechnol.* **2016**, *7*, 2.
71. Thamri, A.; Baccar, H.; Struzzi, C.; Bittencourt, C.; Llobet, E.; Abdelghani, A. VOC Sensing Properties of MHDA-Functionalized Multiwall Carbon Nanotubes. *Procedia Eng.* **2016**, *168*, 268–271. [CrossRef]
72. Wang, F.; Swager, T.M. Diverse Chemiresistors Based upon Covalently Modified Multiwalled Carbon Nanotubes. *J. Am. Chem. Soc.* **2011**, *133*, 11181–11193. [CrossRef] [PubMed]
73. Jiang, L.; Li, S.; Yu, H.; Zou, Z.; Hou, X.; Shen, F.; Li, C.; Yao, X. Amino and thiol modified magnetic multi-walled carbon nanotubes for the simultaneous removal of lead, zinc, and phenol from aqueous solutions. *Appl. Surf. Sci.* **2016**, *369*, 398–413. [CrossRef]

74. Afrin, R.; Shah, N.A.; Abbas, M.; Amin, M.; Bhatti, A.S. Design and analysis of functional multiwalled carbon nanotubes for infrared sensors. *Sens. Actuators A Phys.* **2013**, *203*, 142–148. [CrossRef]
75. Hiroki, A.; Thomas, K.; Franco, C.; William, R.S.; Milo, S.P.S.; Alan, H.W.; Richard, H.F. Work Functions and Surface Functional Groups of Multiwall Carbon Nanotubes. *J. Phys. Chem. B* **1999**, *103*, 8116–8121.
76. Yang, J.; Lee, J.Y.; Too, H.P. Size effect in thiol and amine binding to small Pt nanoparticles. *Anal. Chim. Acta* **2006**, *2*, 206–210. [CrossRef]
77. Cargnello, M.; Wieder, N.L.; Canton, P.; Montini, T.; Giambastiani, G.; Benedetti, A.; Gorte, R.J.; Fornasiero, P. A Versatile Approach to the Synthesis of Functionalized Thiol-Protected Palladium Nanoparticles. *Chem. Mater.* **2011**, *17*, 3961–3969. [CrossRef]
78. Brunet, J.; Genty, E.; Landkocz, Y.; AlZallouha, M.; Billet, S.; Courcot, D.; Siffert, S.; Thomas, D.; De Weireld, G.; Cousin, R. Identification of by-products issued from the catalytic oxidation of toluene by chemical and biological methods. *Comptes Rendus Chim.* **2015**, *18*, 1084–1093. [CrossRef]
79. Casanova-Cháfer, J.; Bittencourt, C.; Llobet, E. Hydrophilicity and carbon chain length effects on the gas sensing properties of chemoresistive, self-assembled monolayer carbon nanotube sensors. *Beilstein J. Nanotechnol.* **2019**, *10*, 565–577. [CrossRef]